Electronic Supplementary Material (ESI) for Green Chemistry.

Selective catalytic tailoring of the H unit in herbaceous lignin for methyl *p*-hydroxycinnamate production over metal-based ionic liquids

Zhangmin Li,[a] Zhenping Cai,[a] Qiang Zeng,[a] Tian Zhang,[a] Liam John France,[a] Changhua Song,[a] Yaqin Zhang,[b] Hongyan He,*[b] Lilong Jiang,[c] Jinxing Long,*[a] and Xuehui Li*[a]

[a] School of Chemistry and Chemical Engineering, State Key Laboratory of Pulp & Paper Engineering, South China University of Technology, Guangzhou 510640, P. R. China.

[b] Beijing Key Laboratory of Ionic Liquids Clean Process, Institute of Process Engineering, Chinese Academy of Sciences, Beijing 100190, P. R. China.

[c] National Engineering Research Centre of Chemical Fertilizer Catalyst, School of Chemical Engineering, Fuzhou University, Fuzhou 350002, Fujian, China.

Contents:

III. Tables & Figures S11

I. Experimental and Analysis Methods

Reagents and biomass sources

Sugarcane bagasse was kindly provided by Guangzhou HUAQIAO sugar factory (Guangzhou, China) and was used as received. Corn stalk, corncob, bamboo, miscanthus, wheat stalk, haulm and pine lignocellulosic biomass sources were obtained from Jiangxi and Henan provinces, China. Metal salts ($CrCl_3$, $FeCl_3$, $CoCl_2·6H_2O$, $NiCl_2·6H_2O$, $CuCl_2$, $ZnCl_2$, $MnCl_2·4H_2O$, $FeBr_3$, $Fe_2(SO_4)_3$, $CrCl_2$, $FeCl_2$ and $FeSO_4·7H_2O$), sodium hydroxide, sulfuric acid, methanol, ethanol, *n*-propanol, *i*-propanol, ethyl acetate and dichloromethane were obtained from Guanghua Chemical Factory Co. Ltd., (Guangdong, China). *N*-methylimidazole, 1-chlorobutane, 1-bromobutane, nitrobenzene, N,O-bis(trimethylsilyl)acetamide dimethyl phthalate, phenethyl 2-phenylacetate, benzyl ether and diphenyl methane were supplied by J&K Technology Co. Ltd., (Beijing, China). All reagents were of analytical grade and used without further purification or pretreatment.

Synthesis of metal-based ionic liquids

ILs 1-butyl-3-methylimidazolium chloride ([Bmim]Cl), 1-butyl-3-methylimidazolium bromine ([Bmim]Br) were synthesized according to previously reported procedures.[1,2] Briefly, 20 mmol 1-chlorobutane or 1-bromobutane was added dropwise to 20 mmol *N*-methylimidazole under intensive stirring at 343 K. After dropwise completed, the mixture was further stirring for 12 h in a nitrogen atmosphere.

The obtained mixture was washed thoroughly with ethyl acetate, the solvent was removed on a rotary evaporator and the sample was dried under vacuum overnight to give [Bmim]Cl and [Bmim]Br, respectively. The MBILs ($[Bmim]_x[MCl_4]$, M=Fe^{2+}, Fe^{3+}, Cr^{3+}, Cr^{2+}, Co^{2+}, Ni^{2+}, Cu^{2+}, Zn^{2+}, Mn^{2+}., x=1, or 2) were synthesized by the combination reaction of IL [Bmim]Cl and metal chloride under dry nitrogen.[3,4] Taking the preparation of $[Bmim][FeCl_4]$ as an example, a typical process is conducted as follows: Mixing 17.47 g IL [Bmim]Cl with 16.25 g $FeCl_3$ (a molar ratio of feedstocks is 1:1) at ambient temperature for 3 h in a nitrogen atmosphere. The obtained MBIL containing solution, exhibiting as a brown-black transparent liquid, was extracted with dichloromethane (2.0 mL× 3). The extracted liquid was treated in a rotary evaporator to remove dichloromethane, before being dried in a vacuum oven at 333 K overnight to yield the final MBIL, [Bmim][$FeCl_4$]. MBILs of the form, [Bmim][MCl_x] and related Br-containing derivatives, were synthesized in a similar manner to that of [Bmim][$FeCl_4$], except where applicable, [Bmim]Br and MBr_x were utilized. $[Bmim]_2[MCl_4]$ type MBILs were synthesized with two molar equivalents of [Bmim]Cl to MCl_2. The physicochemical properties of the aforementioned MBILs are show in Table S11.

Lignin separation from herbaceous biomass

Lignin samples were obtained according to the method used in our previous work.[5] Briefly, 10.0 g herbaceous biomass, 1.2 g H_2SO_4 (98 wt%) and 150 mL 80% aqueous ethanol ($v_{ethanol}/v_{water}$=4: 1) were placed into a 250 mL stainless steel autoclave. The reactor was sealed, purged with nitrogen three times heated to 393 K and held at this temperature for 4.0 h at a stirring speed of 400 rpm. The reactor was cooled rapidly to room temperature under flowing water. The resulting mixture was filtered and the collected solid was thoroughly washed with 80% aqueous ethanol. The washed filtrate and aqueous ethanol washings were collected, mixed with 500 mL deionized water to cause lignin precipitation. The isolated solid was filtered and dried under vacuum at 353 K for 12 h to yield the final lignin feedstock. The total weights obtained from each biomass source are summarized in Table S12.

The separation of MPC

The resulting homogeneous solution generated during reaction was first removed from the autoclave. To minimize losses due to material transfer, the reactor was washed three times (3.0 mL × 3) with anhydrous methanol. The washings were added to the reaction solution and mixed with 80 mL deionized water, resulting in the generation of a muddy colored solution. The solid fraction was separated by consecutive filtration with a 0.22 μm polytetrafluoroethylene membrane, washing with deionized water and drying under vacuum at 333 K until a constant weight is achieved. The resulting solid is the regenerated lignin (Re-lignin), while the filtrate contains a mixture of organic compounds. Subsequent extraction of the filtrate with ethyl acetate (10.0 mL× 3) yields organic and aqueous phases. 2.5 mg dimethyl phthalate (acting as an internal standard) was added to the organic phase, which was diluted to 50 mL (in a volumetric flask) with ethyl acetate. This dilute organic fraction (including the target product, MPC) was qualitatively and quantitatively analyzed with GC-MS-FID. The isolated yield of MPC was obtained on a silica column with a mixed solvent composed of ethyl acetate and petroleum ether ($v_{\text{ethyl acetate}}/v_{\text{petroleum ether}}=1:4$) as eluent. The structure and purity of the isolated MPC was characterized *via* ^{1}H NMR, ^{13}C NMR, ESI-MS, FT-IR and GC-MS-FID respectively. The recycled MBIL catalyst was obtained from the water-soluble fraction after consecutive solvent removal, dichloromethane washing (3.0 mL × 3) and vacuum drying at 353 K overnight.

DFT Calculations

For ionic liquids, the B3LYP method based on density functional theory (DFT) can build a good model and obtain acceptable results to explain or predict experimental phenomena.[6,7] In this work, all structures were optimized using B3LYP method with Gaussian 09 program.[8] The combination basis sets of 6-311+g** and LANL2DZ were employed for atoms (C, H, N, Cl) and metallic atoms (Cr, Fe, Mn, Co, Ni, Cu, Zn), respectively. This combined basis set has been widely used elsewhere for structural optimizations in many areas of research[9-12] and has shown good feasibility in terms of high accuracy requirements and practical computational cost. Subsequently, frequency calculations at the same level verify the predicted structures to be ground states without imaginary frequencies. Then, the binding energies (BE) between cations and anions were computed using eq. (1) and metal-chloride (M-Cl) bonding energies were determined from eq. (2). To further understand the selective cleavage of the ester bond rather than the ether bond in lignin, the interaction between two kinds of model compounds (MCs), phenethyl phenylacetate (representing the model of the ester bond), benzyl ether (representing the model of the ether bond) and these MBILs were calculated. Meanwhile, an implicit solvation model (CPCM)[13,14] was applied to consider the solvation effects of methanol on these optimized geometries. Furthermore, canonical molecular orbital analysis provides an essential understanding of charge transfer and H-bond interactions.[15] The energy gap (ΔE) between anions and MCs were determined using eq. (3), in general, the smaller the ΔE value, the more favorable the reaction,[16] this can be readily explained due to the proportional relationship between ΔE and activation energy, E_a, shows in eq.(4).

$$E_{IE} = E(AB) - E(A) - E(B) \quad (1)$$

$$E_{M-Cl} = E\left([MCl_4]^{n-}\right) - E\left(M^{(4-n)+}\right) - 4 \times E(Cl^-) \quad (2)$$

$$\Delta E = E_{LUMO/anion} - E_{HOMO/MC} \quad (3)$$

$$E_a \propto \Delta E = E_{LUMO} - E_{HOMO} \quad (4)$$

Catalyst characterization analysis

MBIL catalysts were extensively characterized using Fourier transform infrared (FT-IR) spectroscopy, Raman spectroscopy, Thermogravimetric analysis (TGA), Electrospray ionization mass spectrometry (ESI-MS), and Elemental analysis. FT-IR spectra were obtained on a Bruker Tensor 27 spectrophotometer from KBr pellets. Raman spectroscopy was performed on a microscopic confocal Raman spectrometer LabRAM Aramis (Horiba Jobin Yvon), with a 785 nm focused laser beam. TGA was carried out on a NETZSCH STA499C apparatus under a nitrogen atmosphere. The initial oven temperature was set at 303 K, and then ramped at 10 K min^{-1} to 973 K. ESI-MS analysis of MBILs was carried out on an Agilent1290/maXis impact (Bruker). The samples were injected as dilute solutions in methanol, both positive and negative ions were measured with an m/z range of 50 to 1000. C, H and N contents were obtained on a vario EL III elemental analyzer, while metal content was determined on a HITACHI Z-2300 instrument by atomic absorption spectroscopy (AAS). The water content of the resulting MBILs was determined via Karl Fisher titration.

Volatile products identification and measurement

The volatile products were analyzed on an Agilent 7890B gas chromatography apparatus with both mass spectrometry and flame ionization detectors (GC-MS-FID, Agilent 5977A/7890B). Products were qualitatively identified by NIST11 and NIST11s MS libraries, while their contents were quantitatively analyzed *via* an internal standard method using dimethyl phthalate as the standard compound. A HP-5 MS capillary column (30 m × 0.25 mm × 0.25 μm) was used for chemical separation, the oven was held at 323 K for 1.0 min, heated at 10 K min^{-1} to 533 K, where it was held for another 8.0 min. The injector was maintained at 553 K throughout the run, operating in split mode at a 10:1 ratio.

Methods for characterization of original lignin and Re-lignin

Gel permeation chromatography (GPC) analysis

GPC of original lignin and Re-lignin were conducted on an Agilent 1260 high performance liquid chromatography (HPLC) apparatus using a refractive index detector (RID). Tetrahydrofuran (THF) was used as the eluent at a flow rate of 1.0 mL min^{-1} and the column was calibrated using polystyrene standard materials. Lignin and Re-lignin samples were prepared at a concentration of 2.0 mg mL^{-1} in THF; all solutions were filtered through a 0.45 μm filter membrane prior to injection. Investigation of the change in lignin structure after depolymerization reactions was conducted primarily *via* the use of FT-IR and ^{1}H NMR spectroscopies, the latter approach was conducted on a Bruker AVANCE III 400 MHz apparatus (DMSO-d_6 was used as solvent).

2D HSQC NMR spectroscopy analysis

Two-dimensional heteronuclear single quantum coherence (2D HSQC) NMR spectroscopy was recorded on a Bruker Avance III 600 MHz spectrometer. The samples were prepared according to the following procedure; 100 mg lignin was loaded in 1.0 mL DMSO-d_6 and stirred at 323 K for 2.0 h to obtain a thoroughly homogeneous solution and transferred into NMR sample tubes. The ^{1}H, ^{13}C-HSQC experiment was employed in a standard Bruker pulse sequence ‘hsqcetgpsisp’ (phase-sensitive gradient-edited-2D HSQC using adiabatic pulses for inversion and refocusing). 1024 data points (96.1 ms acquisition time) was acquired over a spectral range of 13 ppm in F2 (^{1}H) dimension. 166 ppm spectral range was acquired in the F1 (^{13}C) dimension from 256 data points (7.7 ms acquisition time). 64 scans with 1 s delay at a 90^o pulse. The d_{24} delay was set to 0.87 ms (1/8J, J= 145 Hz). The collected 2D spectrum was processed using Bruker TopSpin 2.1 (Bruker BioSpin) and MestreNova software packages (Mestre Laboratories). The central solvent (DMSO-d_6)

peak served as an internal chemical shift reference point (δ_C/δ_H 39.55/2.49).

Quantitative ^{13}C NMR spectroscopy analysis

Sample were prepared in a similar manner to those analyzed by 2D HSQC. Samples were measured at a frequency of 100.59 MHz with an inverse-gated decoupling sequence, 90° pulse angle, 12 s pulse delay and at a temperature of 323 K. Presented data is the average obtained from 12288 total scans. The spectrum was processed using the same software as 2D HSQC NMR. According to previously reported work,[17] chemical shifts in the 162-157, 123-110 and 110-103.6 ppm range correspond to H, G and S structural units, respectively. Therefore, the ratios of H: G: S were calculated from the integration values of H/2: G/3: S/2.[18-20]

Alkaline nitrobenzene oxidation (ANO) analysis

The procedure for lignin structural unit analysis by ANO was conducted according to the method reported in the literature.[21,22] Typically, lignin (50 mg), sodium hydroxide (2.0 mol L^{-1}, 4.0 mL) and nitrobenzene (0.25 mL) were placed in a 15 mL Teflon autoclave. After heating in an oil bath at 445 K for 2 h, the mixture was diluted with 15 mL deionized water and extracted using CH_2Cl_2 (10.0 mL×3). The resulting aqueous solution was then acidified with 2.0 mol L^{-1} HCl to pH=1, followed by consecutive extraction with CH_2Cl_2 (10.0 mL × 2) and ethyl acetate (5.0 mL×2), respectively. The as-obtained organic phase from the above extraction process was combined and dried with anhydrous Na_2SO_4, followed by rotatory evaporation to remove the mixed solvent. The resulting concentrate was transferred to a vial by 5 mL ethyl ether. The ethyl ether extract was dried at 323 K under nitrogen and subsequently treated with N,O-Bisi(trimethylsilyl)acetamide (150 μL) at 373 K for 10 min. The final products were quantitatively and quantitatively analyzed by GC-MS-FID, using 3, 4, 5-trimethoxybenzaldehyde as the internal standard using the same chromatography column and oven temperature program as described previously for the analysis of the volatile products.

II. Results

Solvent effect

Fig. S9 illustrates the effect of different solvents on lignin depolymerization and ester *p*-hydroxycinnamate (EPC) production. It can be seen that the MPC yield is negligible when lignin depolymerization is conducted in acetone, even though it acts as a good solvent for both lignin and [Bmim][$FeCl_4$], facilitating the formation of a homogenous catalytic system. The addition of 20% (v/v) methanol increases the yield and selectivity of MPC to 34.1 mg g^{-1} and 59.2%, respectively. The alcohol-water mixture is also a conventional solvent for lignin depolymerization,[23,24] which has been reported to exhibit better performance than the individual alcohol.[25] However, this is not the case in this system, lignin conversion does increase but at the expense of MPC yield (Fig. S9). In addition, lower alcohols, such as ethanol, *n*-propanol and *i*-propanol, are effective for selective lignin depolymerization, resulting in the formation of ethyl *p*-hydroxycinnamate (34.4 mg g^{-1}), *n*-propyl *p*-hydroxycinnamate (28.4 mg g^{-1}) and *i*-propyl *p*-hydroxycinnamate (16.3 mg g^{-1}) as the major products, respectively. However, it should be noted that lignin conversion and EPC yield decreases with either an increase in carbon chain length or branching degree. EPC selective production from bagasse lignin (a *p*-hydroxycinnamate structural unit[26,27]) occurs *via* transesterification with alcohol, therefore, the alcohol acts as both reagent and solvent. As such, process efficiency increases with alcohols of a lower carbon number or branching degree, which matches observations made for previously reported transesterification reactions.[28,29]

Quantitative ^{13}C NMR analysis and alkaline nitrobenzene oxidation

Quantitative ^{13}C NMR spectroscopy (Fig. S11) and alkaline nitrobenzene oxidation (ANO) (Table S4) were carried out to gain a more comprehensive understanding of the change in lignin structural unit concentrations during the selective lignin depolymerization process. It has been demonstrated in previous studies that chemical shifts between 162-157, 123-110 and 110-103.6 ppm can be assigned to the H, G and S structural units of lignin, respectively.[20,27,30] The results listed in Table S4 demonstrate that original lignin has an H: G: S ratio of 15:45:40, while it changes to 4:45:51 after the reaction. Namely, the concentration of the H unit decreases significantly from 15 to 4% when lignin is treated with the $[Bmim][FeCl_4]$ catalytic system, meaning that 86.0 wt% of H structure unit of bagasse lignin was converted. At the same time, most of the G and S units are reserved in Re-lignin. This result can be further confirmed by the ANO, another traditional method for measurement of the concentration of structural units in lignin,[21,22] where the relative mass ratios of H: G: S in the original lignin are determined to be 15: 47: 38 and 5: 40: 55 prior to and after the depolymerization process, respectively. Both approaches clearly exhibit a small degree of variation in absolute terms, but both corroborate our findings from other methods, that this approach exhibits extremely high preference towards the transformation of H units.

Reusability of catalyst $[Bmim][FeCl_4]$

Under optimized conditions (1.0 mmol catalyst, 10.0 mL methanol, 420 K and 6.0 h for 0.25 g of bagasse lignin), the reusability of the best performing MBIL catalyst, $[Bmim][FeCl_4]$ was investigated. It is found to possess rather good recycling stability as demonstrated in Fig. S14, where satisfactory lignin conversion and MPC selectivity of 42.4% and 66.1%, respectively is still apparent after five consecutive reactions. In order to investigate the reason behind the slight loss in conversion and selectivity, elemental analysis, FT-IR spectroscopy, Raman spectroscopy and TGA were conducted. Elemental analysis (Table S8) indicates that there is an increase in the C, H and N content of the catalyst after cycling the catalyst, while an obvious decrease in Fe concentration (detected by atomic absorption spectroscopy) is found. Comparative analysis of the C and N contents (C/N) reveals that there is a subsequent increase in the former, suggesting that C-rich compounds accumulate on the catalyst. FT-IR spectroscopy, demonstrates that there is little difference between features associated with [Bmim][$FeCl_4$] prior to and after reaction, suggesting that the ionic liquids structure is mostly preserved. However, the presence of a number of new absorption features (3355, 1742, 1030 and 846 cm^{-1}) are consistent with observations made by numerous authors[27,31,32] and may be attributed to residual lignin (Fig. S15). Furthermore, Raman spectra (Fig. S16) exhibit considerable comparative changes in the band near 1600 cm^{-1} before and after reaction. The feature in question correlates closely to the symmetric stretching mode of aryl rings, suggesting that they are related to structures associated to lignin.[33] The presence of deposited lignin can be further confirmed by TGA, where the recovered [Bmim][$FeCl_4$] catalyst demonstrates a lowering of the decomposition onset temperature and a higher residual weight, at 973 K (Fig. S17). Thus, the slight loss in conversion and selectivity may be attributed to losses associated with leaching of [$FeCl_4$]$^-$ and due to the presence of lignin remnants complexed with the MBIL.

III. Tables & Figures

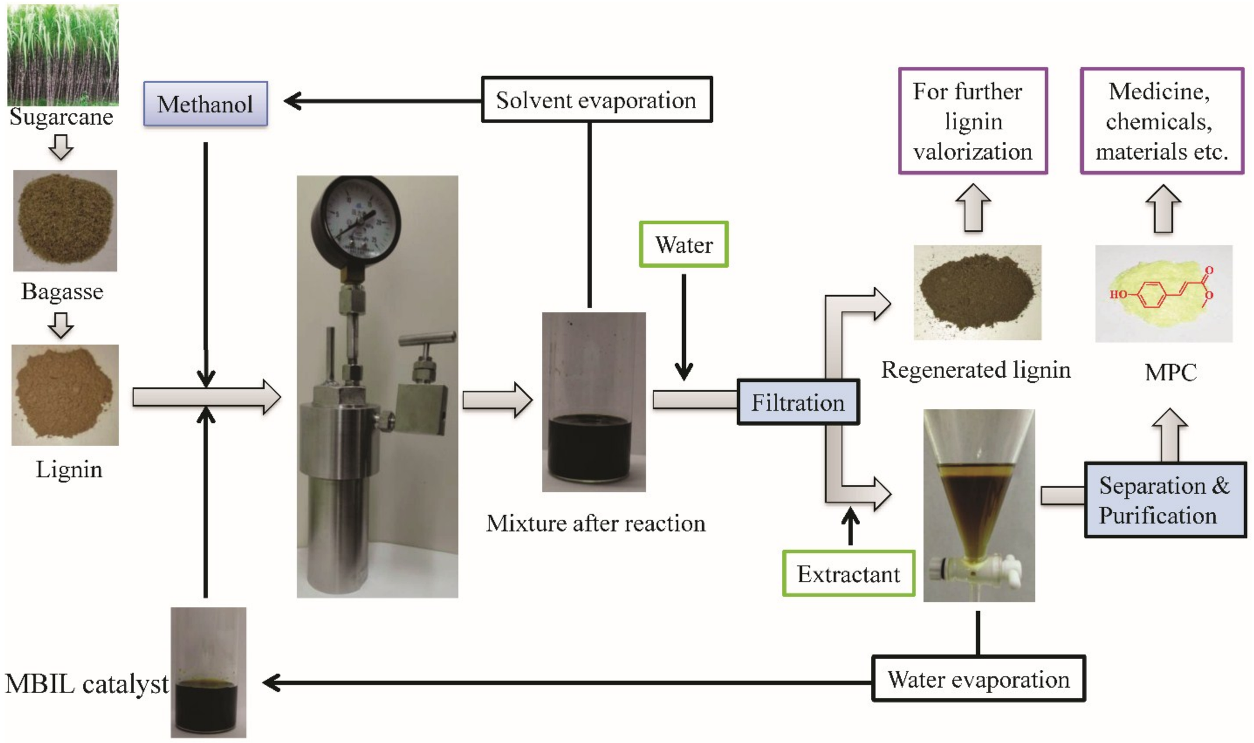

Scheme S1 Schematic representation of the proposed integrated lignin biorefinery process.

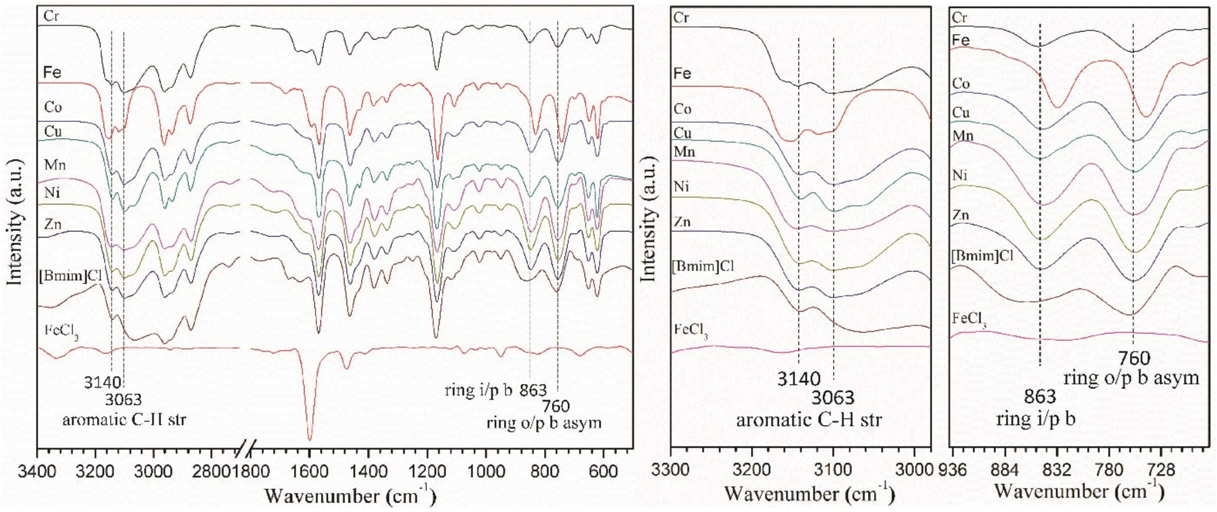

Fig. S1. FT-IR spectra of MBIL catalysts (Metal=Cr, Fe, Co, Cu, Mn, Ni, Zn), IL [Bmim]Cl and $FeCl_3$ with partial magnification of a specific wavenumber region between 700-900 and 3000-3300 cm^{-1}.

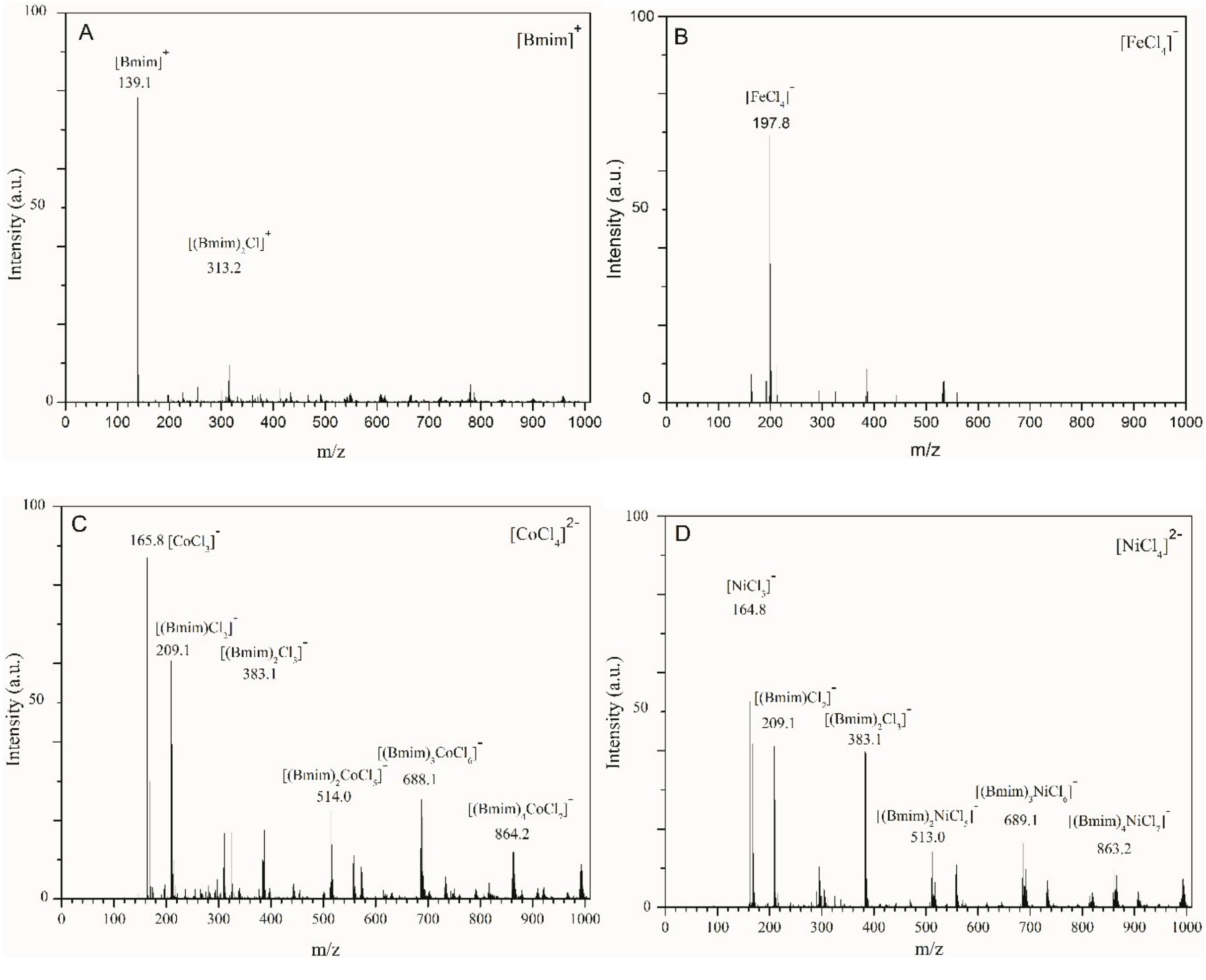

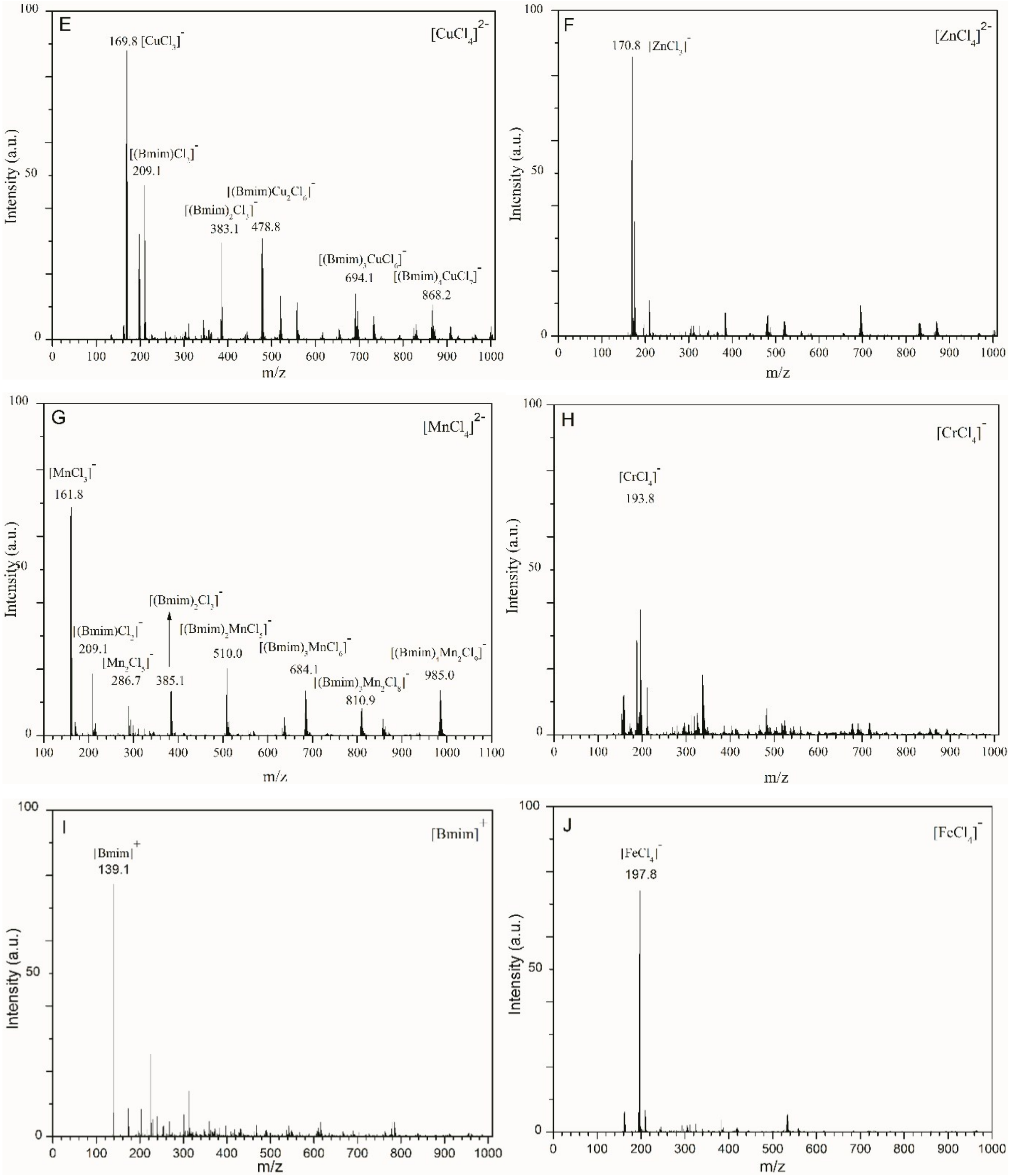

Fig. S2. ESI-MS signals for [Bmim]$^+$ (A), [FeCl$_4$]$^-$ (B), [CoCl$_4$]$^{2-}$ (C), [NiCl$_4$]$^{2-}$ (D), [CuCl$_4$]$^{2-}$ (E), [ZnCl$_4$]$^{2-}$ (F), [MnCl$_4$]$^{2-}$ (G), [CrCl$_4$]$^-$ (H) and [Bmim][FeCl$_4$] after 5 reactions conducted under optimized conditions (I and J).

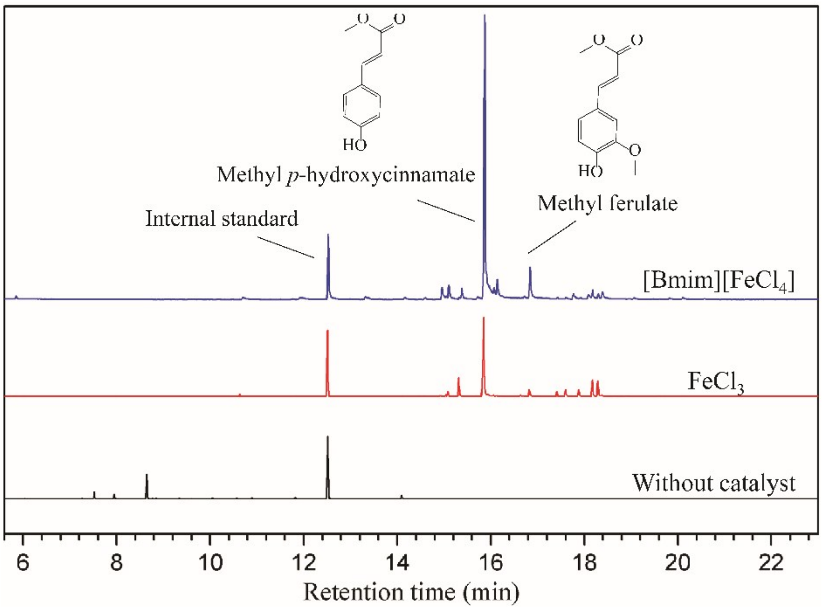

Fig. S3. GC-MS analysis of the volatile product fraction generated from selective lignin conversion with $FeCl_3$ and [Bmim][$FeCl_4$] and without catalysts.

Table S1. List of volatile products identified *via* GC-MS analysis

Product classification	RT (min)	Compound	Structure	Formula	Percentage (wt%)[a]
Aliphatic compounds (4.9 wt%)					
	3.27	1,1-dimethoxypropan-2-one	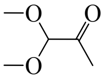	$C_5H_{10}O_3$	1.9
	5.04	1,1,2,2-tetramethoxyethane	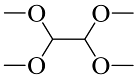	$C_6H_{14}O_4$	1.7
	10.69	3,6-dimethyl-2,3,3a,4,5,7a-hexahydrobenzofuran	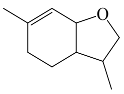	$C_{10}H_{16}O$	1.3
Phenolic monomers (95.1 wt%)					
H unit	15.87	Methyl *p*-hydroxycinnamate	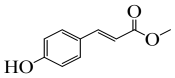	$C_{10}H_{10}O_3$	70.5
G units	11.91	Vanillin	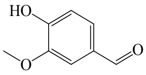	$C_8H_8O_3$	1.7
	13.31	Methyl vanillate	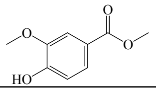	$C_9H_{10}O_4$	1.3

Table S1. List of volatile products identified *via* GC-MS analysis (Continued)

Product classification	RT (min)	Compound	Structure	Formula	Percentage (wt%)[a]
G units	14.15	Isovanillin	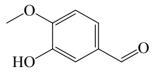	$C_8H_8O_3$	0.9
	14.59	(E)-4-(3-hydroxyprop-1-en-1-yl)-2-methoxyphenol	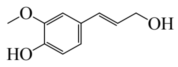	$C_{10}H_{12}O_3$	0.6
	15.10	3-Hydroxy-4-methoxyphenylacetic acid	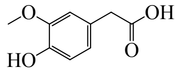	$C_9H_{10}O_4$	3.2
	15.38	Methyl 2-(3,4-dimethoxyphenyl)-2-hydroxyacetate	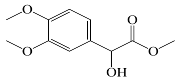	$C_{11}H_{14}O_5$	2.1
	15.71	2-Hydroxy-1-(4-hydroxy-3-methoxyphenyl)ethanone	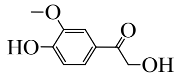	$C_9H_{10}O_4$	1.0
	16.83	Methyl ferulate	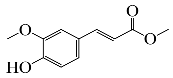	$C_{11}H_{12}O_4$	6.7
S units	14.94	Syringaldehyde	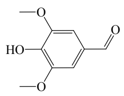	$C_9H_{10}O_4$	4.0
	16.13	methyl 2-(4-hydroxy-3,5-dimethoxyphenyl)acetate	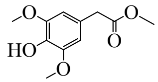	$C_{11}H_{14}O_5$	2.4
Others	9.41	2,3-dihydrobenzofuran	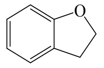	C_8H_8O	0.2
	15.05	1-(2,6-dihydroxy-4-methoxyphenyl)ethanone	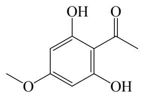	$C_9H_{10}O_4$	0.5

[a] [Bmim][$FeCl_4$] as catalyst (Table 1, entry 8).

Reaction conditions: 0.25 g bagasse lignin, 1.0 mmol [Bmim][$FeCl_4$], 10.0 mL methanol, 420 K, 6.0 h.

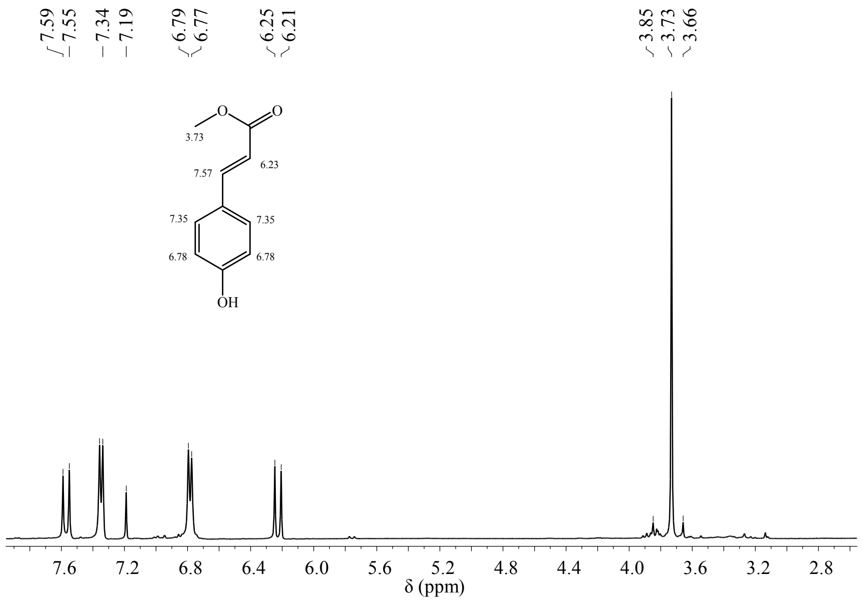

Fig. S4. ^{1}H NMR spectrum of purified MPC.

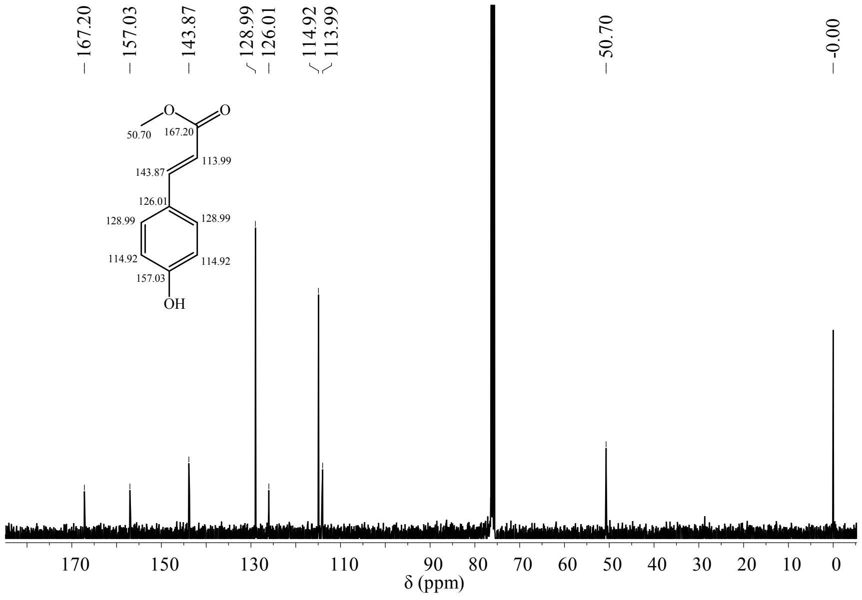

Fig. S5. ^{13}C NMR spectrum of purified MPC.

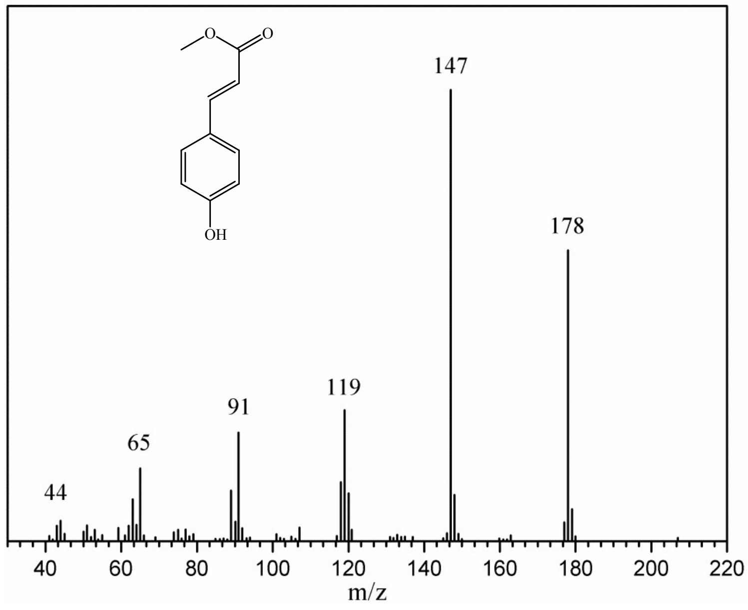

Fig. S6. ESI-MS spectrum of purified MPC.

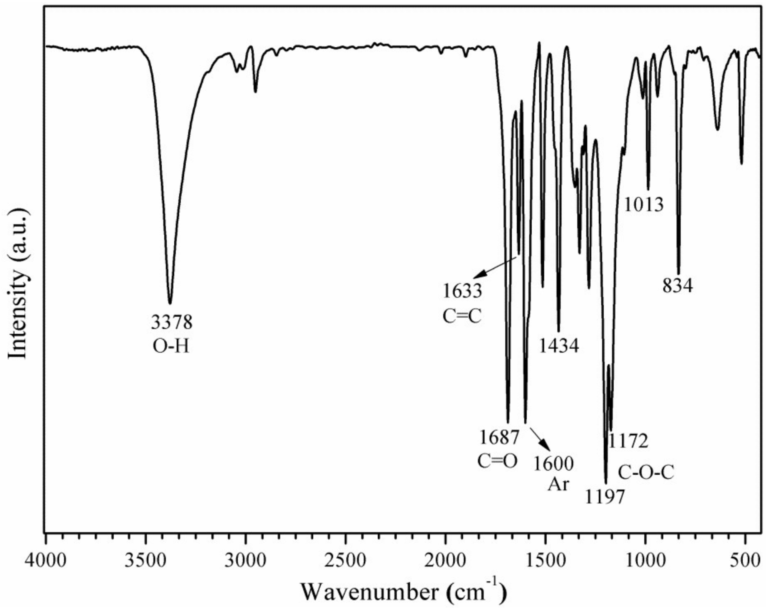

Fig. S7. FT-IR spectrum of purified MPC.

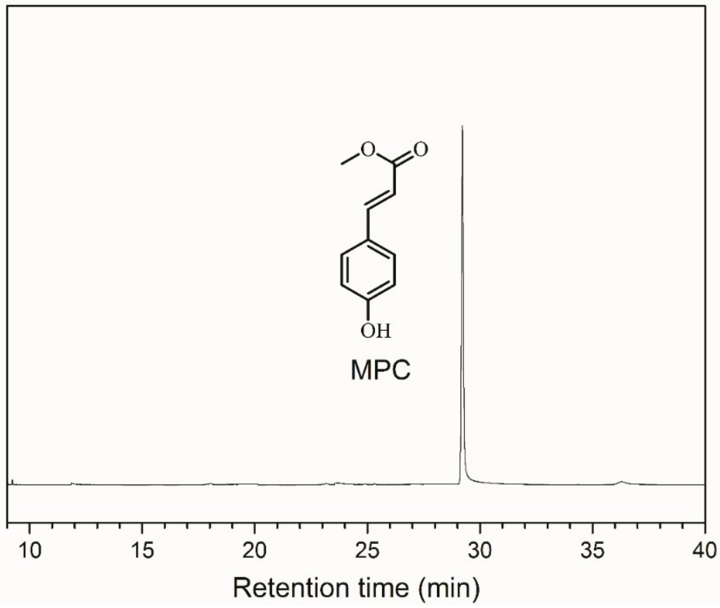

Fig. S8. GC-FID chromatogram of purified MPC.

^{1}H NMR (400 MHz, $CDCl_3$) δ = 7.57 (1H, d, *J* = 16.0 Hz, =CH), 7.35 (2H, d, *J* = 8.4 Hz, ArH), 6.78 (2H, d, *J* = 8.4 Hz, ArH), 6.23 (1H, d, *J* = 16.0 Hz, =CH), 3.73 (3H, s, CH_3). ^{13}C NMR (101 MHz, $CDCl_3$) δ = 167.20, 157.03, 143.87, 128.99, 126.01, 114.92, 113.99, 50.70. ESI-MS (m/z): 178 (M^+, 75%), 147 (100%), 119 (40%). FT-IR (KBr, cm^{-1}), 3378 (O-H), 1687 (C=O), 1633 (C=C), 1197 (C-O-C), 1172 (C-O-C).

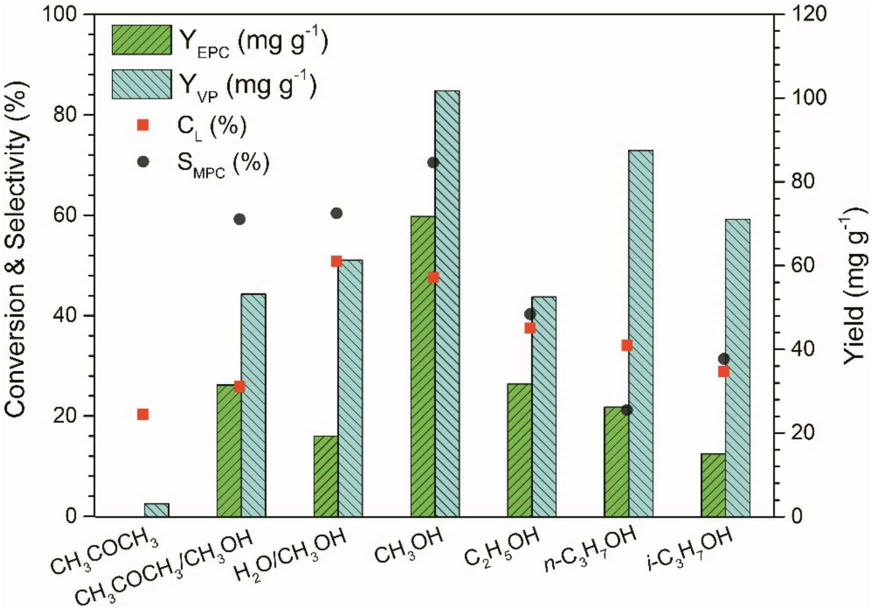

Fig. S9. Solvent effect for selective lignin depolymerization.

(Reaction conditions: 0.25 g lignin, 1.0 mmol [Bmim][$FeCl_4$], 10.0 mL solvent, 420 K, 6.0 h.)

Table S2. Assignments of the 2D HSQC spectra of the lignin fractions

Lable	δ_C/δ (ppm)[a]	δ_C/δ (ppm)[b]	Assignments
C_β	50.5/3.75	50.5/3.75	C_β-H_β in phenylcoumaran (C)
OCH_3	55.9/3.74	56.6/3.13	C-H in methoxyls
B_γ	59.9/4.02	ND	C_γ-H_γ in cinnamyl alcohol end-groups (B)
A-S_γ	61.7/3.64	60.2/3.53	C_γ-H_γ in β-O-4 substructures (A-S)
A-$S_{\gamma(\gamma\text{-}p\mathrm{CA})}$	64.5/4.19	ND	C_γ-H_γ in γ-*p*CA of β-O-4 (A-S)
A_α	72.1/4.91	ND	C_α-H_α in β-O-4 unit (A)
A-H/G_β	83.1/4.41	82.6/4.39	C_β-H_β in β-O-4 substructures (A-H/G)
A-$S_{\beta(\gamma\text{-}p\mathrm{CA})}$	80.6/4.49	ND	C_β-H_β in γ-*p*CA of β-O-4 (A-S)
$S_{2,6}$	104.6/6.71	105.0/6.60	$C_{2,6}$-$H_{2,6}$ in syringyl units (S)
G_2	111.8/6.96	112.2/6.93	C_2-H_2 in guaiacyl units (G)
G_5	115.9/6.94	115.6/6.91	C_5-H_5 in guaiacyl units (G)
G_6	120.2/6.79	120.6/6.77	C_6-H_6 in guaiacyl units (G)
$H_{2/6}$	129.2/7.25	129.2/7.20	$C_{2,6}$-$H_{2,6}$ in H units (H)
$p\mathrm{CA}_{3/5}$	116.1/6.81	116.0/6.79	$C_{3,5}$-$H_{3,5}$ in *p*-coumarate (*p*CA)
$p\mathrm{CA}_{2/6}$	130.7/7.46	130.6/7.52	$C_{2,6}$-$H_{2,6}$ in *p*-coumarate (*p*CA)
$p\mathrm{CA}_7$	145.2/7.42	145.1/7.54	C_7-H_7 in *p*-coumarate (*p*CA)
$p\mathrm{CA}_8$	114.5/6.27	114.4/6.37	C_8-H_8 in *p*-coumarate (*p*CA)
FA_2	112.0/7.30	112.1/7.29	C_2-H_2 in ferulate (FA)
FA_7	145.2/7.33	145.1/7.37	C_7-H_7 in ferulate (FA)
FA_8	114.4/6.11	114.9/6.25	C_8-H_8 in ferulate (FA)

[a] δ_C/δ_H (ppm), the chemical shift of original lignin; [b] δ_C/δ_H (ppm), the chemical shift of Re-lignin generated under optimized conditions; ND: Not detected; Signals were assigned by comparison according to literature values.[30, 36-38]

Table S3. FT-IR vibrational wavenumbers and the assignments observed for lignin

Wavenumbers (cm^{-1})	Vibrational assignment
3438	O-H stretching
2933	C-H stretching
1603	C-C, C=C (aromatic skeleton), stretching
1516	C-C, C=C (aromatic skeleton), stretching
1466	C-H (CH_3 + CH_2), bending
1325	C-O (syringyl unit) stretching
1269	C-O (guaiacyl unit) stretching
1217	C-OH (phenolic OH) stretching
1169	C=O stretching of *p*-hydroxyphenyl structures
1120	C-H aromatic in-plain stretching
1030	C-H aromatic in-plain stretching
835	C-H aromatic out-plain stretching

The obtained spectrum is found to be consistent with herbaceous lignin.[27, 34, 35]

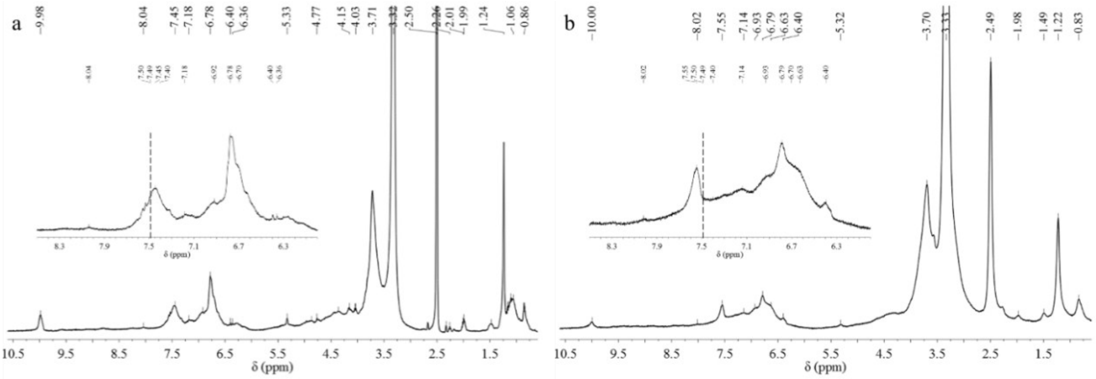

Fig. S10. ^{1}H NMR spectra of original lignin (a) and Re-lignin obtained after catalytic conversion under optimized conditions (b).

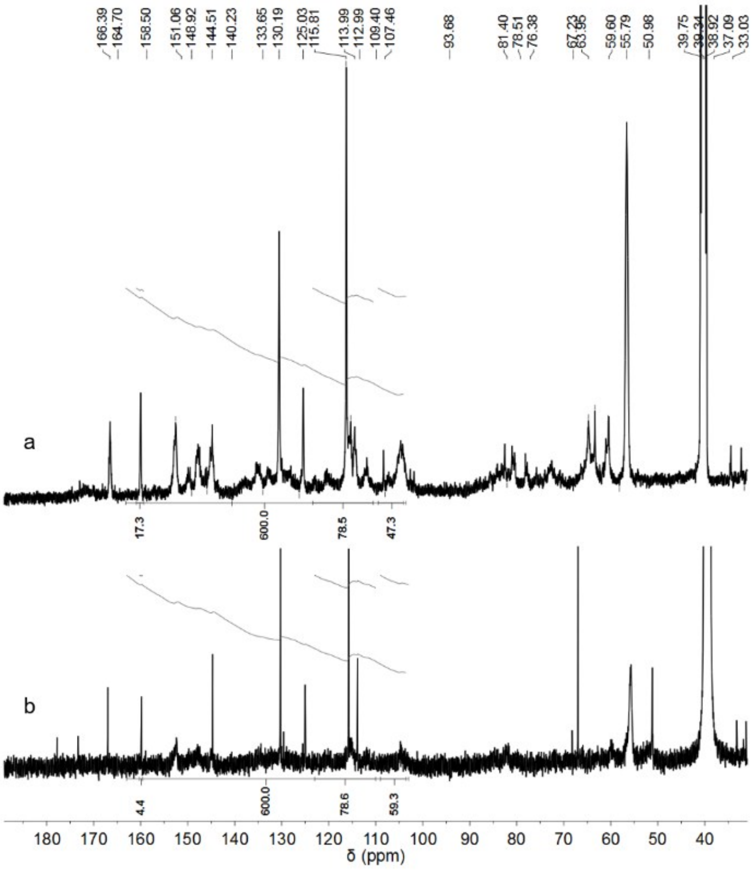

Fig. S11. Quantitative ^{13}C NMR spectra of original (a) and Re-lignin after catalytic conversion under optimized conditions (b).

Table S4. Comparative analysis of the structural unit content of original lignin and Re-lignin

Lignin unit	phenolic acids and aldehydes	Lignin fraction (%)	
		original lignin	Re-lignin[a]
H	*p*-hydroxybenzaldehyde	5.15	2.08
	p-hydroxybenzoic acid	0.13	Trace
	p-hydroxycoumaric acid	4.56	Trace
G	vanillin	24.67	12.28
	vanillic acid	0.20	0.04
	acetovanillone	1.86	4.18
	ferulic acid	5.22	0.13
S	syringaldehyde	17.22	17.17
	syringic acid	0.51	0.83
	acetosyringone	7.37	4.64
H: G: S	Total	66.89	41.35
	ANO[b]	15: 47: 38	5: 40: 55
	NMR[c]	15: 45: 40	4: 45: 51

[a] Re-lignin was generated under optimized conditions.

[b]. ratio of H: G: S determined using the ANO method.

[c] ratio of H: G: S determined using the ^{13}C NMR method.

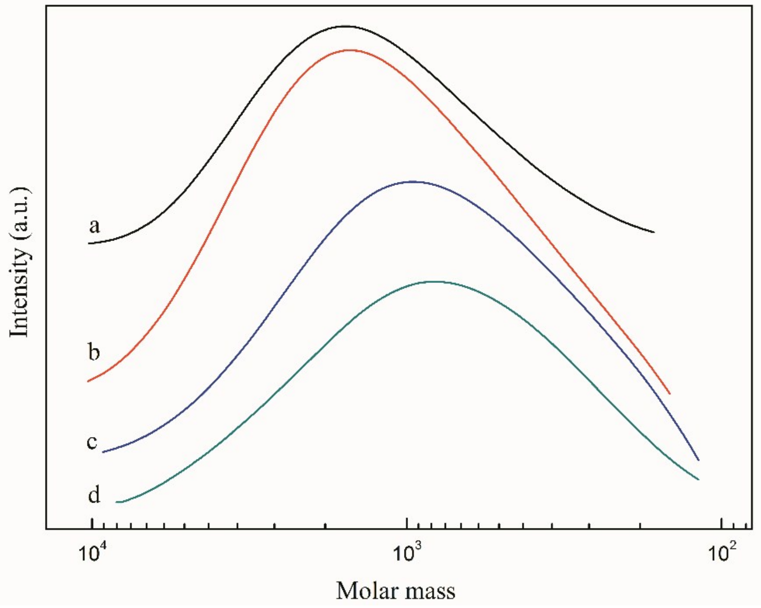

Fig. S12. Molecular weight distribution of original lignin (a) and Re-lignin generated without catalyst (b), with $FeCl_3$ (c) and [Bmim][$FeCl_4$] (d) under optimized conditions.

Table S5. Average molar mass of original lignin and Re-lignin generated with and without catalyst

Catalyst	Sample	molecular weight (g mol^{-1})		
		M_w	M_n	D
-	original lignin	1860	1010	1.84
Without catalyst	Re-lignin A	1986	960	2.07
$FeCl_3$	Re-lignin B	1472	637	2.19
[Bmim][$FeCl_4$]	Re-lignin C	1299	603	2.16

In all cases, Re-lignin was generated under optimized conditions. M_w (weight-average molecular weights), M_n (number-average molecular weights), D=M_w/M_n (polydispersities).

Table S6. Elements analysis of original lignin and Re-lignin[a]

Samples	Catalyst	Elemental content					Experimental molecular formula	Degree of unsaturation	HHV (MJ kg^{-1})[c]
		C	H	O[b]	N	S			
Raw lignin	-	60.88	5.80	31.90	0.62	0.80	$C_9H_{10.3}O_{3.5}N_{0.08}S_{0.04}$	4.85	23.17
Re-lignin A	No catalyst	64.29	6.34	28.35	0.67	0.36	$C_9H_{10.7}O_{3.0}N_{0.08}S_{0.02}$	4.65	25.73
Re-lignin B	[Bmim]Cl	63.09	5.80	30.18	0.54	0.40	$C_9H_{9.9}O_{3.2}N_{0.07}S_{0.02}$	5.05	24.23
Re-lignin C	$FeCl_3$	64.13	5.72	34.90	0.67	0.31	$C_9H_{9.6}O_{3.1}N_{0.08}S_{0.02}$	5.20	23.63
Re-lignin D	[Bmim][$FeCl_4$]	64.37	6.61	28.30	0.67	0.50	$C_9H_{11.1}O_{3.0}N_{0.08}S_{0.03}$	4.95	24.85

[a] In all cases, Re-lignin was generated under optimized conditions, and the sample was dried under vacuum at 333 K for 24 h.

[b] The content of oxygen was estimated by the conservation of mass, based on the assumption that the sample only contains C, H, O, N and S.

[c] Evaluated by Dulong Formula: HHV (MJ Kg^{-1}) =0.3383 × C + 1.422 × (H - O/8).

Table S7. Selective depolymerization of different lignin sources[a]

Entry	Lignin	H units (%)[b]	C_L (%)	Y_{VP} (mg g^{-1})			S_{MPC} (%)
				Y_{MPC}	Y_{others}	Total	
1	Corncob	17.1	53.7	90.9	26.9	117.8	72.4
2	Bagasse	14.8	47.6	77.7	32.5	110.2	70.5
3	Bamboo	10.2	72.9	55.2	43.4	98.6	56.0
4	Miscanthus	9.1	55.8	48.2	39.7	87.9	54.8
5	Corn stalk	7.9	55.4	31.8	24.0	55.8	57.0
6	Wheat stalk	5.6	48.8	6.2	23.4	29.6	21.0
7	Haulm	5.0	40.5	4.7	25.8	30.5	24.1
8	Pine sawdust	-	32.5	-	1.2	1.2	-

[a] In all cases [Bmim][$FeCl_4$] and optimized reaction conditions were used.

[b] Determined by quantitative ^{13}C NMR.

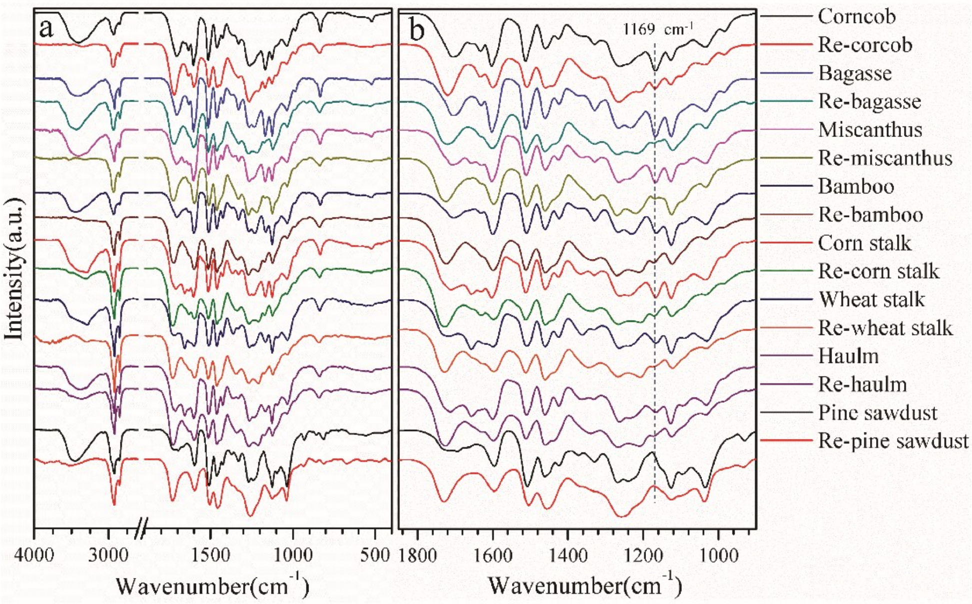

Fig. S13. FT-IR spectra of different sources of original lignin and Re-lignin (a) and expanded region from 1000 to 1800 cm^{-1} (b) (Band at 1169 cm^{-1} relates to H unit in lignin).

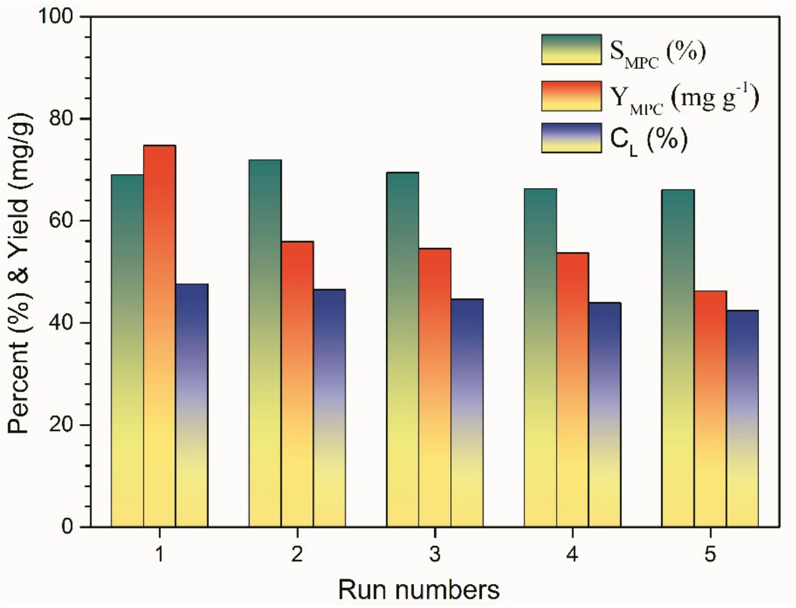

Fig. S14 Reusability of [Bmim][$FeCl_4$] tested under optimized conditions.

Table S8. Elemental analysis of fresh and used [Bmim][$FeCl_4$]

[Bmim][$FeCl_4$]	Elemental composition (wt%)					Total composition
	C	H	N	C/N	Fe[a]	(wt%)
Calculated	28.52	4.49	8.32	3.43	16.58	41.33
Found	26.55	4.45	8.42	3.15	14.21	39.42
After recycled 5 times	31.24	5.11	9.38	3.33	13.31	45.73

Recycled catalyst has been exposed to 5 consecutive reactions conducted under optimized conditions.

[a] Detected by atomic absorption spectroscopy.

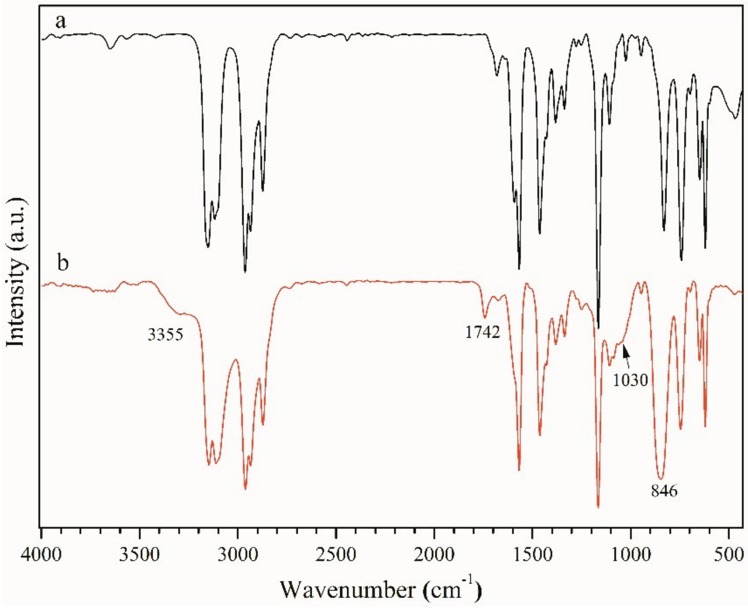

Fig. S15. FT-IR spectra of [Bmim][FeCl$_4$] before (a) and after 5 reactions conducted under optimized conditions (b).

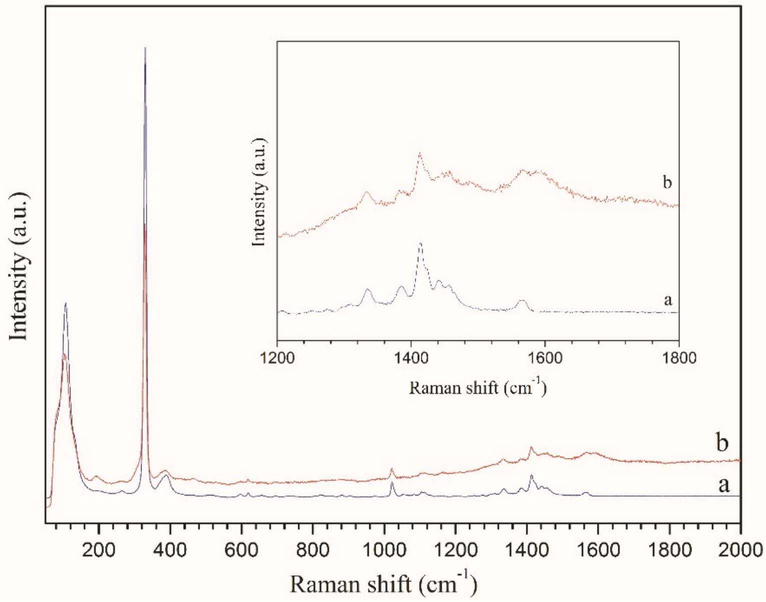

Fig. S16. Raman spectra of [Bmim][FeCl$_4$] before (a) and after 5 reactions conducted under optimized conditions (b).

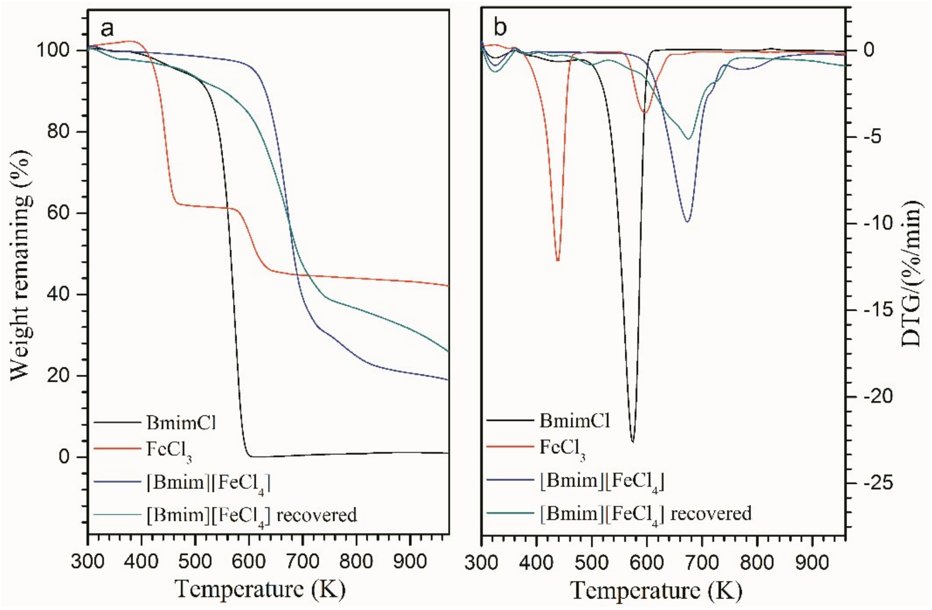

Fig. S17. TGA (a) and DTG (b) curves of [Bmim]Cl, $FeCl_3$, fresh [Bmim][$FeCl_4$] and after 5 reactions conducted under optimized conditions.

Table S9. Determination of the energy gap between the HOMO of the model ester compound and the LUMO of different anionic complexes

Sort	LUMO (au)		HOMO (au)		Δ*E* (au)		Δ*E* (au)
	α	β	α	β	α	β	
$CoCl_4^{2-}$	0.1842	0.1843	0.0154	0.0262	**0.4376**	0.4377	**0.4376**
$CrCl_4^-$	-0.0037	0.0492	-0.1215	-0.1539	**0.2497**	0.3026	**0.2497**
$CuCl_4^{2-}$	0.1850	0.1274	0.0192	0.0224	0.4384	**0.3809**	**0.3809**
$FeCl_4^-$	0.0879	-0.0064	-0.1590	-0.1533	0.3413	**0.2470**	**0.2470**
$MnCl_4^{2-}$	0.1806	0.1808	0.0206	0.0059	**0.4340**	0.4342	**0.4340**
$NiCl_4^{2-}$	0.1846	0.1778	0.0156	0.0247	0.4381	**0.4313**	**0.4313**
$ZnCl_4^{2-}$	0.1822		0.0111		0.4357	**0.2534**	**0.2534**
Ester-MC	-0.0299		-0.2534				

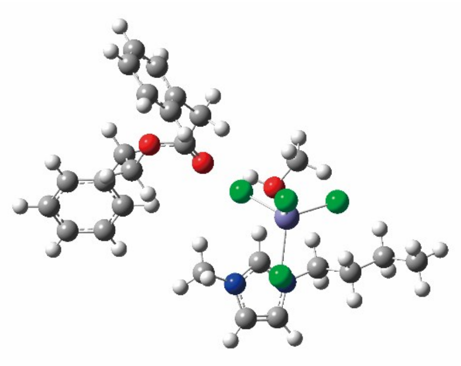

[Bmim]-[$FeCl_4$]-MeOH-Ester
-30.38 kJ/mol

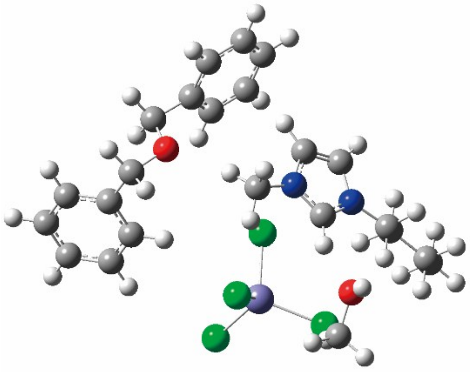

[Bmim]-[$FeCl_4$]-MeOH-Ether
-28.65 kJ/mol

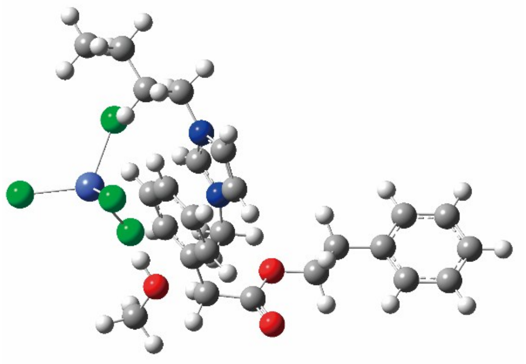

[Bmim]-[$CoCl_4$]-MeOH-Ester
-26.48 kJ/mol

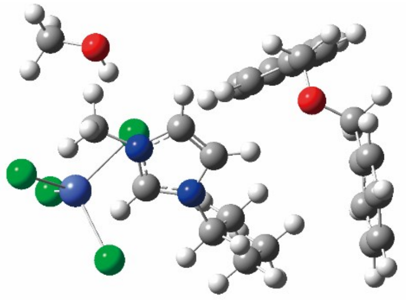

[Bmim]-[$CoCl_4$]-MeOH-Ether
-21.88 kJ/mol

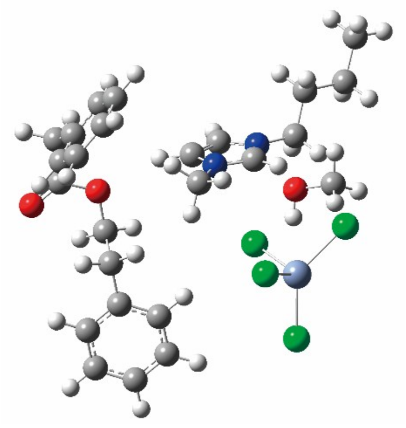

[Bmim]-[$CrCl_4$]-MeOH-Ester
-18.83 kJ/mol

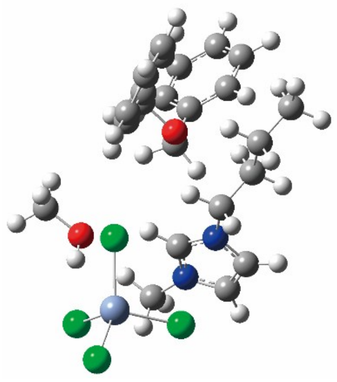

[Bmim]-[$CrCl_4$]-MeOH-Ether
-12.38 kJ/mol

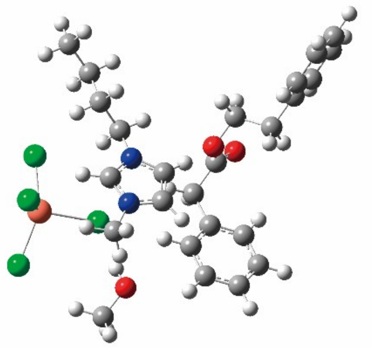

[Bmim]-[$CuCl_4$]-MeOH-Ester

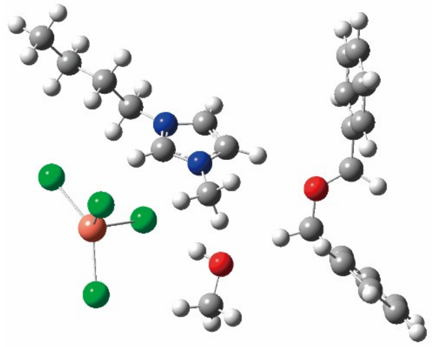

[Bmim]-[$CuCl_4$]-MeOH-Ether

-27.30 kJ/mol

-21.33 kJ/mol

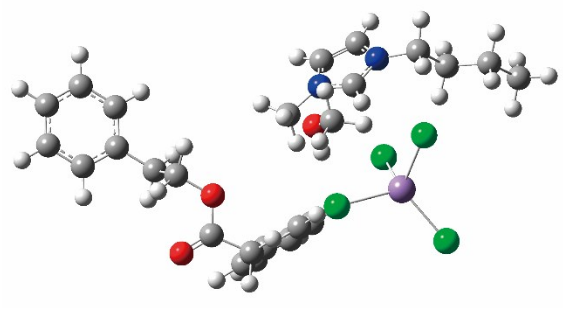

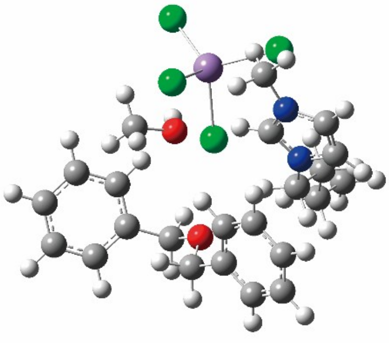

[Bmim]-[MnCl$_4$]-MeOH-Ester
-29.14 kJ/mol

[Bmim]-[MnCl$_4$]-MeOH-Ether
-21.64 kJ/mol

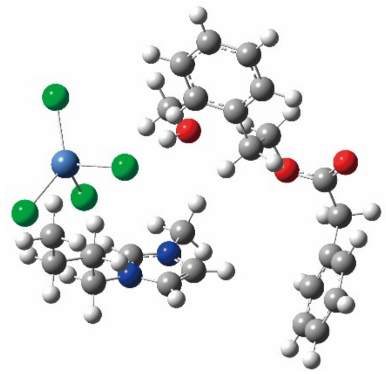

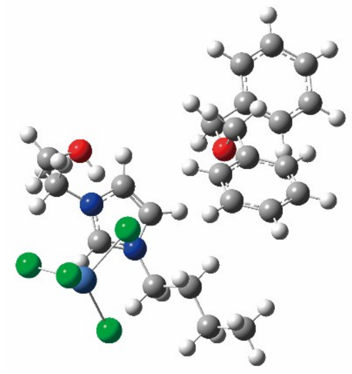

[Bmim]-[NiCl$_4$]-MeOH-Ester
-29.15 kJ/mol

[Bmim]-[NiCl$_4$]-MeOH-Ether
-16.33 kJ/mol

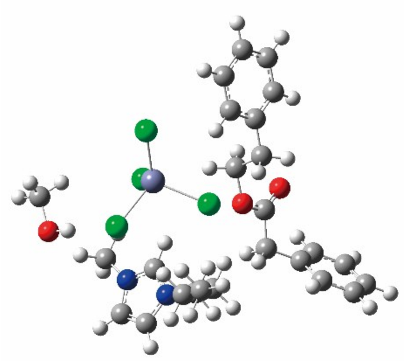

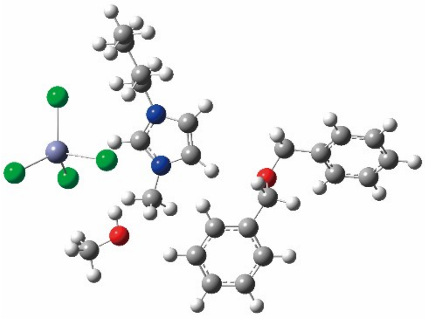

[Bmim]-[ZnCl$_4$]-MeOH-Ester
-37.75 kJ/mol

[Bmim]-[ZnCl$_4$]-MeOH-Ether
-23.38 kJ/mol

Fig. S18. Optimized MBIL-methanol-MC liquid phase structures and binding energies of the predicted ester (phenethyl phenylacetate) and ether (benzyl ether) complexes.

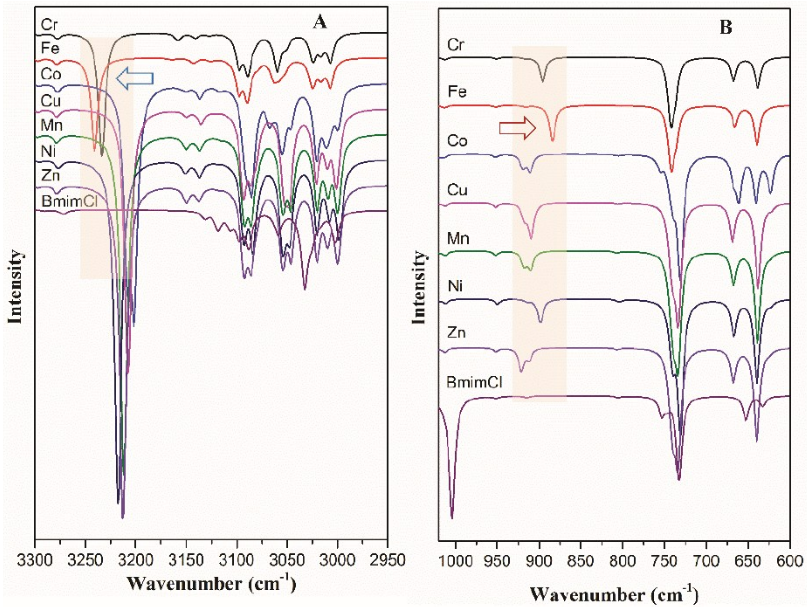

Fig. S19. Calculated frequencies of IR active aromatic C-H stretches (A) and fingerprint peaks associated with imidazolium (B) obtained from frequency analysis using a scaling factor of 0.963.

Table S10. Summary of M-Cl bond energies and lengths

$[MCl_4]^{n-}$	$E([MCl_4]^{n-})$ kJ/mol	$E(M^{(4-n)+})$ kJ/mol	E(M-Cl) kJ/mol	Length(M-Cl) Å
$[FeCl_4]^-$	-1964.64	-121.30	-1395.92	2.262
$[CrCl_4]^-$	-1927.51	-84.18	-1388.94	2.258
$[MnCl_4]^{2-}$	-1945.15	-103.04	-590.74	2.479
$[CoCl_4]^{2-}$	-1986.26	-144.07	-637.54	2.396
$[NiCl_4]^{2-}$	-2010.46	-168.28	-636.84	2.389
$[CuCl_4]^{2-}$	-2037.28	-195.06	-653.70	2.390
$[ZnCl_4]^{2-}$	-1906.78	-64.63	-618.50	2.422

Table S11. Physicochemical properties of MBILs

MBILs	Calculated or found	Elemental composition (wt%)			Total composition (wt%)	Purity (wt%)[a]	Water content (wt%)
		C	H	N			
$[Bmim][FeCl_4]$	Calculated	28.52	4.49	8.32	41.33	98.81	0.057
	Found	26.55	4.45	8.42	39.42		
$[Bmim][CrCl_4]$	Calculated	28.85	4.54	8.41	41.80	98.59	0.063
	Found	28.9	4.54	8.53	41.97		
$[Bmim]_2[CoCl_4]$	Calculated	40.10	6.31	11.69	58.10	97.37	0.023
	Found	40.86	6.35	11.39	58.60		
$[Bmim]_2[NiCl_4]$	Calculated	40.10	6.31	11.70	58.11	96.77	0.074
	Found	39.09	6.48	12.09	57.66		
$[Bmim]_2[CuCl_4]$	Calculated	39.72	6.25	11.58	57.55	98.42	0.110
	Found	39.64	6.64	11.40	57.68		
$[Bmim]_2[ZnCl_4]$	Calculated	39.57	6.23	11.54	57.34	97.79	0.031
	Found	40.68	6.51	11.29	58.48		
$[Bmim]_2[MnCl_4]$	Calculated	40.44	6.36	11.79	58.59	95.39	0.085
	Found	40.29	6.64	11.27	58.20		

[a] The purity was calculated according to N content in MBILs.

Table S12. Total weight of lignin separated from herbaceous biomass sources [a]

Entry	Herbaceous source	Weight of separated lignin (g)	Lignin fraction (wt%) [b]
1	Corncob	1.2	12
2	Bagasse	1.6	16
3	Bamboo	1.6	16
4	Miscanthus	1.5	15
5	Corn stalk	1.7	17
6	Wheat stalk	1.7	17
7	Haulm	1.9	19
8	Pine sawdust	2.2	22

[a] Separation conditions: 10.0 g raw biomass, 1.2 g H_2SO_4, 150.0 mL aqueous ethanol, 393 K, 4.0 h; data are the average of three replicants. [b] Lignin fraction = (weight of separated lignin / weight of biomass) × 100%.

References

1. L. M. Ramenskaya, E. P. Grishina, A. M. Pimenova and M. S. Gruzdev, *Russ. J. Phys. Chem. A+*, 2008, **82**, 1098-1103.
2. P. Bonhôte, A.-P. Dias, N. Papageorgiou, K. Kalyanasundaram and M. Grätzel, *Inorg. Chem.*, 1996, **35**, 1168-1178.
3. Q. Wang, Y. Geng, X. Lu and S. Zhang, *ACS Sustain. Chem. Eng.*, 2015, **3**, 340-348.
4. M. D. Nguyen, L. V. Nguyen, E. H. Jeon, J. H. Kim, M. Cheong, H. S. Kim and J. S. Lee, *J. Catal.*, 2008, **258**, 5-13.
5. J. X. Long, X. H. Li, B. Guo, L. F. Wang and N. Zhang, *Catal. Today*, 2013, **200**, 99-105.
6. H. Y. He, H. Chen, Y. Z. Zheng, S. J. Zhang and Z. W. Yu, *Chem. Eng. Sci.*, 2015, **121**, 169-179.
7. X. Meng, H. He, Y. Nie, X. Zhang, S. Zhang and J. Wang, *ACS Sustain. Chem. Eng.*, 2017, **5**, 3081-3086.
8. M. J. Frisch, G. W. Trucks, H. B. Schlegel, G. E. Scuseria, M. A. Robb, J. R. Cheeseman, G. Scalmani, V. Barone, B. Mennucci, G. A. Petersson, H. Nakatsuji, M. Caricato, X. Li, H. P. Hratchian, A. F. Izmaylov, J. Bloino, G. Zheng, J. L. Sonnenberg, M. Hada, M. Ehara, K. Toyota, R. Fukuda, J. Hasegawa, M. Ishida, T. Nakajima, Y. Honda, O. Kitao, H. Nakai, T. Vreven, J. A. Montgomery Jr, J. E. Peralta, M. J. Bearpark, J. Heyd, E. N. Brothers, K. N. Kudin, V. N. Staroverov, R. Kobayashi, J. Normand, K. Raghavachari, A. P. Rendell, J. C. Burant, S. S. Iyengar, J. Tomasi, M. Cossi, N. Rega, N. J. Millam, M. Klene, J. E. Knox, J. B. Cross, V. Bakken, C. Adamo, J. Jaramillo, R. Gomperts, R. E. Stratmann, O. Yazyev, A. J. Austin, R. Cammi, C. Pomelli, J. W. Ochterski, R. L. Martin, K. Morokuma, V. G. Zakrzewski, G. A. Voth, P. Salvador, J. J. Dannenberg, S. Dapprich, A. D. Daniels, J. B. Foresman, J. V. Ortiz, J. Cioslowski and D. J. Fox, *Gaussian 09, Revision D. 01, Gaussian, Inc., Wallingford CT,*, 2013.
9. Y. Q. Zhang, H. Y. He, K. Dong, M. H. Fan and S. J. Zhang, *RSC Adv.*, 2017, **7**, 12670-12681.
10. G. B. Damas, A. B. Dias and L. T. Costa, *J. Phys. Chem. B*, 2014, **118**, 9046-9064.
11. Z. W. Qu and G. J. Kroes, *J. Phys. Chem. B*, 2006, **110**, 8998-9007.
12. C. E. Check, T. O. Faust, J. M. Bailey, B. J. Wright, T. M. Gilbert and L. S. Sunderlin, *J. Phys. Chem. A*, 2001, **105**, 8111-8116.

13. C. J. Cramer and D. G. Truhlar, *Chem. Rev.*, 1999, **99**, 2161-2200.
14. X. Wei, Y. Wang, A. J. Hernández-Maldonado and Z. Chen, *Green Energ. Environ.*, 2017, **2**, 363-369.
15. K. Dong, Y. Song, X. Liu, W. Cheng, X. Yao and S. Zhang, *J. Phys. Chem. B*, 2012, **116**, 1007-1017.
16. T. Tsuchimochi and G. E. Scuseria, *J. Chem. Phys.*, 2010, **133**, 141102-141106.
17. T. Q. Yuan, S. N. Sun, F. Xu and R. C. Sun, *J. Agric. Food. Chem.*, 2011, **59**, 10604-10614.
18. R. Obst John and J. Ralph, *Holzforschung*, 1983, **37**, 297-302.
19. D. V. Evtuguin, C. P. Neto, A. M. Silva, P. M. Domingues, F. M. Amado, D. Robert and O. Faix, *J. Agric. Food. Chem.*, 2001, **49**, 4252-4261.
20. E. A. Capanema, M. Y. Balakshin and J. F. Kadla, *J. Agric. Food. Chem.*, 2005, **53**, 9639-9649.
21. K. Iiyama and T. B. T. Lam, *J. Sci. Food Agric.*, 1990, **51**, 481-491.
22. E. Billa, M.-T. Tollier and B. Monties, *J. Sci. Food Agric.*, 1996, **72**, 250-256.
23. T. Klamrassamee, N. Laosiripojana, D. Cronin, L. Moghaddam, Z. Zhang and W. O. Doherty, *Bioresour. Technol.*, 2015, **180**, 222-229.
24. J. Zakzeski, A. L. Jongerius, P. C. Bruijnincx and B. M. Weckhuysen, *ChemSusChem*, 2012, **5**, 1602-1609.
25. J. Long, W. Lou, L. Wang, B. Yin and X. Li, *Chem. Eng. Sci.*, 2015, **122**, 24-33.
26. R. C. Sun, X. F. Sun and S. H. Zhang, *J. Agric. Food. Chem.*, 2001, **49**, 5122-5130.
27. J. X. Sun, X. F. Sun, R. C. Sun, P. Fowler and M. S. Baird, *J. Agric. Food. Chem.*, 2003, **51**, 6719-6725.
28. J. Li and Z. Guo, *ChemSusChem*, 2017, **10**, 1792-1802.
29. P. K. Sahoo and L. M. Das, *Fuel*, 2009, **88**, 1588-1594.
30. J. L. Wen, S. L. Sun, B. L. Xue and R. C. Sun, *Materials*, 2013, **6**, 359-391.
31. J. L. Wen, B. L. Xue, F. Xu and R. C. Sun, *Bioenerg. Res.*, 2012, **5**, 886-903.
32. S. Nanayakkara, A. F. Patti and K. Saito, *ACS Sustain. Chem. Eng.*, 2014, **2**, 2159-2164.
33. Z. Ji, J. F. Ma, Z. H. Zhang, F. Xu and R. C. Sun, *Ind. Crop. Prod.*, 2013, **47**, 212-217.
34. X. M. Zhang, T. Q. Yuan, F. Peng, F. Xu and R. C. Sun, *Sep. Sci. Technol.*, 2010, **45**, 2497-2506.

35. B. Strzemiecka, L. Klapiszewski, A. Jamrozik, T. J. Szalaty, D. Matykiewicz, T. Sterzynski, A. Voelkel and T. Jesionowski, *Materials*, 2016, **9**, 517-530.
36. A. Rahimi, A. Azarpira, H. Kim, J. Ralph and S. S. Stahl, *J. Am. Chem. Soc.*, 2013, **135**, 6415-6418.
37. A. Rahimi, A. Ulbrich, J. J. Coon and S. S. Stahl, *Nature*, 2014, **515**, 249-252.
38. C. S. Lancefield, O. S. Ojo, F. Tran and N. J. Westwood, *Angew. Chem. Int. Ed.*, 2015, **54**, 258-262.